



HAL
open science

Introducing Thermal Inertia for Monitoring Snowmelt Processes With Remote Sensing

R. Colombo, R. Garzonio, B. Di Mauro, M. Dumont, F. Tuzet, S. Cogliati, G. Pozzi, A. Maltese, E. Cremonese

► **To cite this version:**

R. Colombo, R. Garzonio, B. Di Mauro, M. Dumont, F. Tuzet, et al.. Introducing Thermal Inertia for Monitoring Snowmelt Processes With Remote Sensing. *Geophysical Research Letters*, 2019, 46 (8), pp.4308-4319. 10.1029/2019GL082193. meteo-03657894

HAL Id: meteo-03657894

<https://meteofrance.hal.science/meteo-03657894v1>

Submitted on 3 May 2022

HAL is a multi-disciplinary open access archive for the deposit and dissemination of scientific research documents, whether they are published or not. The documents may come from teaching and research institutions in France or abroad, or from public or private research centers.

L'archive ouverte pluridisciplinaire **HAL**, est destinée au dépôt et à la diffusion de documents scientifiques de niveau recherche, publiés ou non, émanant des établissements d'enseignement et de recherche français ou étrangers, des laboratoires publics ou privés.

Copyright

Geophysical Research Letters

RESEARCH LETTER

10.1029/2019GL082193

Key Points:

- Snow thermal inertia resembles the different phases of snowmelt processes
- An empirical model is proposed for estimating snow density from apparent thermal inertia
- This study may open new perspectives in remote sensing of snowmelt processes

Supporting Information:

- Supporting Information S1
- Figure S1
- Figure S2
- Figure S3
- Figure S4
- Data Set S1

Correspondence to:

R. Garzonio and B. Di Mauro,
roberto.garzonio@unimib.it;
biagio.dimauro@unimib.it

Citation:

Colombo, R., Garzonio, R., Di Mauro, B., Dumont, M., Tuzet, F., Cogliati, S., et al. (2019). Introducing thermal inertia for monitoring snowmelt processes with remote sensing. *Geophysical Research Letters*, *46*, 4308–4319. <https://doi.org/10.1029/2019GL082193>

Received 24 JAN 2019



Accepted 20 MAR 2019

Accepted article online 25 MAR 2019

Published online 24 APR 2019

©2019. American Geophysical Union.
All Rights Reserved.

Introducing Thermal Inertia for Monitoring Snowmelt Processes With Remote Sensing

R. Colombo¹, R. Garzonio¹ , B. Di Mauro¹, M. Dumont², F. Tuzet^{2,3}, S. Cogliati¹ , G. Pozzi¹, A. Maltese⁴, and E. Cremonese⁵

¹Earth and Environmental Sciences Department, University of Milano-Bicocca, Milan, Italy, ²University Grenoble Alpes, Université de Toulouse, Météo-France, CNRS, CNRM, Centre d'Etudes de la Neige, Grenoble, France, ³UGA/CNRS, Institut des Géosciences de l'Environnement (IGE), Saint Martin d'Heres, France, ⁴Engineering Department, University of Palermo, Palermo, Italy, ⁵Environmental Protection Agency of Aosta Valley, Aosta, Italy

Abstract Thermal inertia has been successfully used in remote sensing applications that span from geology, geomorphology to hydrology. In this paper, we propose the use of thermal inertia for describing snow dynamics. Two different formulations of thermal inertia were tested using experimental and simulated data related to snowpack dynamics. Experimental data were acquired between 2012 and 2017 from an automatic weather station located in the western Italian Alps at 2,160 m. Simulations were obtained using the one-dimensional multilayer Crocus model. Results provided evidences that snowmelt phases can be recognized, and average snowpack density can be estimated reasonably well from thermal inertia observations ($R^2 = 0.71$; RMSE = 65 kg/m³). The empirical model was also validated with manual snow density measurements ($R^2 = 0.80$; RMSE = 54 kg/m³). This study is the first attempt at the exploitation of thermal inertia for snow monitoring, combining optical and thermal remote sensing data.

Plain Language Summary Alpine snow represents a fundamental reservoir of fresh water at midlatitude. Remote sensing offers the opportunity to estimate snow properties in different spectral domains. In particular, the knowledge of the spatial and temporal variability of snow density could allow modeling of the snow water equivalent, which knowledge is crucial for managing water resources in the face of current climate change. In this study we show for the first time that snow thermal inertia can contribute to monitoring of snowmelt processes and snow density, opening new perspectives for remote sensing of the cryosphere.

1. Introduction

The cryosphere is an important constituent of planet Earth, since it regulates short wave radiation balance and stores fresh water essential for human societies and ecosystems. During the climatic history of Earth, the cryosphere has played a fundamental role in defining the global air temperature through complex feedback mechanisms with the atmosphere and the biosphere. To date, the study of the cryosphere is an active field of research, because its components are extremely sensitive to global climate changes (Beniston et al., 2018; Immerzeel et al., 2010). The retreat of mountain glaciers and the negative mass balance of ice sheets have become emblematic of the effect of natural and anthropogenic climate changes on natural environments (Huss et al., 2017; Oerlemans, 1994). Alpine snowpack is strongly variable in time and space due to their complex interactions with the overlying atmosphere and the underlying ground. The knowledge of snowmelt processes and the snow water equivalent is of crucial importance in alpine areas for understanding water availability and for defining water management strategies (Beniston et al., 2003, 2018). A large part of the cryosphere components exists very close to their limit of phase transition from solid to liquid. For this reason, the study of melting dynamics represents a fundamental task of current scientific research, in particular, in the framework of current increase of atmospheric temperature.

In the context of snowmelt processes, the evolution of the snowpack is determined by the energy and mass balance equations (Dingman, 2015). In general, the melting period of a seasonal snowpack begins when the net input of energy becomes increasingly positive, and it can be ideally separated in three phases (Dingman, 2015): (i) warming phase: during which absorbed energy results in increasing temperature, until the snowpack is isothermal at 0 °C and a significant increase of snow density occurs (McCreight & Small,

2014); (ii) ripening phase: during which energy is used for melting, increasing the liquid water content, but the meltwater is retained in the snowpack by surface tension forces until the snow reaches its liquid holding capacity (Williams & Tarboton, 1999); and (iii) output phase: during which further input of energy produces meltwater output. During these phases, the optical, thermal, and physical properties of snow strongly change. In alpine areas, this variability can also occur quickly due to complex topography. Snow is a complex porous medium made of air and up to three phases of water: ice, water vapor, and liquid water. Their relative proportion controls optical and thermal properties, while weather conditions control metamorphism and compaction (Calonne et al., 2011; Haeberli & Whiteman, 2014; Pomeroy & Brun, 2001).

Remote sensing offers the opportunity to estimate snow properties in the optical, thermal, and microwave domain (Dozier & Painter, 2004; Hall & Martinec, 2012; Nolin, 2010; Tedesco, 2014). Overall, optical data are focused on grain size, snow cover extent, surface albedo, and light absorbing particles (LAPs; Bormann et al., 2018; Dozier & Painter, 2004; Green et al., 2002; Kokhanovsky et al., 2018; Painter et al., 2013; Skiles et al., 2018). Thermal data are instead used to map snow/ice surface temperature and spectral emissivity (Aubry-Wake et al., 2015). Finally, active and passive microwave data contribute to determine spectral emissivity, wet or dry snow, snow liquid water content, and liquid water column, snow depth, snow density, and overall snow water equivalent (Kelly et al., 2003; Lacroix et al., 2009; Leduc-Leballeur et al., 2017; Naderpour & Schwank, 2018; Schellenberger et al., 2012; Stiles & Ulaby, 1980; Ulaby & Stiles, 1980). Frozen components of the Earth feature very peculiar optical and thermal properties. Snow and ice crystals reflect most of the radiation in visible wavelengths (reflectance >0.9) and absorb radiation in near-infrared and short-wave infrared (Kokhanovsky & Zege, 2004; Warren, 1982). Regarding thermal properties, snow has a very high emissivity (>0.9) in the 8–12 μm spectral range behaving like a black body. Thermal properties of snow vary primarily with density, which is related to changes in microstructure and liquid water content (Arenson et al., 2015; Calonne et al., 2011; Dacic et al., 2013). Surface processes that promote snow and ice melting are mainly driven by net radiation (including shortwave and longwave radiation). Changes in air temperature first induce warming of the snowpack, then a phase transition (i.e., snow melting) results in the disappearance of snow at midlatitudes. Increases in air temperature also induce structural changes in snow and the coarsening of the snow microstructure. This increase in the dimension of crystals is involved in a feedback mechanism that promotes further melting, since large grains are characterized by a lower albedo (Warren & Wiscombe 1980). The albedo of snow is also influenced by the LAPs content (Painter et al., 2012; Di Mauro et al., 2015, 2017; Liou et al., 2014; He et al., 2018), and the interaction of non-ice material with snow may alter its thermal properties by decreasing the emissivity and enhancing surface temperature. This process directly feeds the phase transition from solid to liquid and accelerates the disappearance of snow in spring (Painter et al., 2007), which impacts the availability of water for ecosystem functioning, irrigation, hydropower, etc. (Skiles et al., 2018).

Although optical, thermal and radar remote sensing has been widely used at field, airborne and satellite levels (König et al., 2001), no combination of thermal and optical data has ever been pursued to infer snow properties and to monitor the snowmelt phases. The detection of snowmelt phases represents valuable information that could be assimilated in snow/hydrological models. Overall, the knowledge of different snowmelt phases may help to evaluate the impact of climate change on cryosphere components. Beside other properties, snow density is an essential variable for quantifying the amount of water contained within the snowpack (i.e., snow water equivalent) and the water availability at catchment scale (Jonas et al., 2009; Molotch et al., 2005; Sturm et al., 2010). Several attempts to retrieve snow density were conducted using active (Shi & Dozier, 2000; Snehmani et al., 2010; Thakur et al., 2012) and passive microwave remote sensing (Champollion et al., 2018; Lacroix et al., 2009; Lemmetyinen et al., 2016; Naderpour et al., 2017; Roy et al., 2017; Schwank et al., 2015; Schwank & Naderpour, 2018). However, the possibility to get accurate estimates of snow density from remote sensing still represents a great challenge.

In this context, we hypothesize that remotely sensed thermal inertia can be a useful indicator of snowmelt properties and overall for snow monitoring. Thermal inertia is a physical property of the surfaces, which determines resistance to temperature change under seasonal and diurnal heating (Nearing et al., 2012). Thermal inertia is described as: $P = \sqrt{k\rho c}$, and is expressed in $\text{J}\cdot\text{m}^{-2}\cdot\text{K}^{-1}\cdot\text{s}^{1/2}$, where ρ is the density (kg/m^3), k is the thermal conductivity ($\text{J}\cdot\text{m}^{-1}\cdot\text{s}^{-1}\cdot\text{K}^{-1}$), and c is the specific heat ($\text{J}\cdot\text{kg}^{-1}\cdot\text{K}^{-1}$). If thermal inertia changes in space and time, it could be possible to generate maps that can be used to monitor snowmelt and

snow parameters. For snow hydrology purposes, this quantity has been only peripherally investigated in the context of the NASA Heat Capacity Mapping Mission (HCMM; Short and Stuart, 1982) in terms of apparent thermal inertia. This study qualitatively indicated that higher values of apparent thermal inertia may define the extent of melting snow at the lowest elevations, while medium and low values likely represent drier, colder snow at the highest elevations. The authors concluded that further study would be needed to determine whether these data actually provide information useful for snowmelt prediction. However, to our knowledge, no further quantitative studies on apparent thermal inertia and snowmelt has been conducted since that time, although this variable has been extensively used to discriminate surface planetary geology and urban heat island assessment (Ait-Mesbah et al., 2015; Brenning et al., 2012; Cracknell & Xue, 1996; Gaitani et al., 2017; Mitra & Majumdar, 2004; Price, 1977; Putzig & Mellon, 2007; Wang et al., 2010; Xue & Cracknell, 1995). Moreover, many studies have demonstrated that it can be used to estimate soil moisture (Kahle et al., 1976; Kang et al., 2017; Maltese et al., 2012, 2013; Minacapilli et al., 2009; Price, 1980; Tian et al., 2015; Van Doninck et al., 2011; Verhoef, 2004; Verstraeten et al., 2006).

Since changes of snow density and liquid water content continuously occur in the snowpack, spatial and temporal patterns of thermal inertia can theoretically reveal snowmelt processes. The main goal of this study is to understand if snow thermal inertia can be an indicator of temporal evolution of snowmelt processes and to evaluate its relationship with snow parameters, with particular attention to snow density. This study is a first attempt to interpret this process in a snowpack, and it may open new perspectives for detection of snowmelt processes and snow parameters from remote sensing observations.

2. Data and Methods

First, we define a theoretical formulation of snow thermal inertia, then we exploit experimental data and snow modeling outputs to compare the seasonal series of apparent thermal inertia with snowmelt processes. Finally, we analyze the relationships between thermal inertia and snow variables considering both simulated and field measurements data.

2.1. Experimental Site

The test site is located in the northwestern Italian Alps (Aosta Valley, IT) at an altitude of 2,160 m a.s.l. (45°50'40"N, 7°34'41"E). The site is a subalpine unmanaged grassland area, classified as intraalpine with semicontinental climate. It extends over an almost flat area (i.e., slope lower than 5°) of about 150 × 200 m, and it is generally covered by snow from the end of October to late May. This natural ecosystem has been under continuous investigation since 2009 to evaluate how vegetation phenology and snowpack respond to current climatic conditions (Galvagno et al., 2013; Julitta et al., 2014; Migliavacca et al., 2011). The experimental site belongs to the ICOS (Integrated Carbon Observation System) Phenocam and LTER (Long-Term Ecosystem Research in Europe) networks, and it is equipped with an automatic weather station and eddy covariance flux tower for continuous measurements of snow parameters and heat fluxes. Hourly measurements of several parameters are therefore available during the whole year. A full description of the instruments is reported in Galvagno et al. (2013).

2.2. Snow Thermal Inertia Modeling

The snow thermal inertia P_s has been modeled according to the following considerations: (i) the snowpack density (ρ_s , kg/m³) can be considered as the combination of dry snow and liquid water content (Dadic et al., 2013); (ii) the thermal conductivity of the snowpack can be inferred from snow density [Calonne et al., 2011]; (iii) the specific heat capacity of snow (c_s) can be modeled using the relative fraction of ice, water, and air in the snowpack and considering their specific heat capacities (Sergienko et al., 2008; Verseghy, 1991).

$$P_s = \sqrt{(2.5 \cdot 10^{-6} \rho_s^2 - 1.23 \cdot 10^{-4} \rho_s + 0.024) \cdot \rho_s \cdot \left(c_i \frac{\rho_s - \theta \rho_w}{\rho_i} + c_w \theta + c_a \left(1 - \frac{\rho_s - \theta \rho_w}{\rho_i} - \theta \right) \right)} \quad (1)$$

$[\text{J m}^{-2} \text{K}^{-1} \text{s}^{-1/2}]$

where c_i , c_w , c_a are the specific heat capacities of ice, water, and air, respectively; ρ_i , ρ_w ; are their densities, and θ is the mass liquid water content (%) normalized between 0 and 1. The derivation of P_s is presented in the Supporting Information S1.

Equation (1) allows computing snow thermal inertia and it represents the baseline for interpreting the spatial and temporal variability of apparent thermal inertia, which can be instead estimated using remote sensing data (section 2.3). P_s was computed for hydrological years 2012–2017 using simulated snow parameters (i.e., density and liquid water content) by Crocus model (section 2.4).

2.3. Estimation of the Snow Apparent Thermal Inertia

The apparent thermal inertia of snow (AP_s) has been computed using the formulation proposed by Xue and Cracknell (1995) and Maltese et al. (2013), and it is based on the solution of the one-dimensional (1-D) thermal diffusion equation, using a first-order approximation of a Fourier series under the hypothesis that surface temperature has a sinusoidal cosine behavior (Maltese, Bates, et al., 2013). Using data recorded at the experimental site for 2012–2017 hydrological years, AP_s was calculated as follows:

$$AP_s = \frac{(1-\alpha)SW_{in}}{\Delta T_{(t_2-t_1)}} \frac{A_1 \cos(\omega t_1 - \delta_1) - \cos(\omega t_2 - \delta_1)}{\sqrt{\omega} \sqrt{1 + \frac{1}{b} + \frac{1}{2b^2}}} \quad \left[\text{J m}^{-2} \text{K}^{-1} \text{s}^{-1/2} \right] \quad (2)$$

where α is the snow shortwave broadband albedo (–) averaged between 13:00 and 15:00 (local time: UTC +1), ΔT (K) is the surface temperature difference between the nighttime and the daytime temperatures measured at times t_1 (4:00 and 6:00) and t_2 (13:00 and 15:00), respectively; SW_{in} is the daily average shortwave incoming radiation (W/m^2); ω is the angular velocity of Earth rotation (rad/s); A_1 and b are the coefficients of a first-order approximation of the Fourier series (for details, see Maltese, Bates, et al., 2013), while δ_1 (rad) is the phase difference between surface temperature and shortwave incoming radiation that can be retrieved straightforward under the hypothesis that the time at which surface temperature reaches the maximum value is known (Xue & Cracknell, 1995). Shortwave broadband albedo in the range of 400–2,800 nm was measured by a net radiometer (Kipp and Zonen, cnr4, uncertainty <5%), while surface snow temperature was measured by a SI-111 thermal sensor (Apogee, uncertainty ± 0.2 °C). Albedo values ≥ 1 and surface temperature differences ≤ 0 were discarded, and residual AP_s outliers were removed using the Median Absolute Deviation approach with a moving kernel of 10 days.

2.4. Snowpack Modeling

Snowpack variables were simulated using the one-dimensional multilayer Crocus model, which reproduce the evolution of the snowpack (Brun et al., 1989; Essery et al., 1999; Tuzet et al., 2017; Vionnet et al., 2012). In this model snow dynamics are represented as a function of energy and mass transfer between the snowpack, the atmosphere, and ground below. We used a specific Crocus version that makes use of the Two-stream Analytical Radiative TransFER in Snow (TARTES; Libois et al., 2013) radiative transfer model (Tuzet et al., 2017). In this study, we performed Crocus simulation accounting for the impact of LAPs (dust and black carbon), further details can be found in Di Mauro et al. (2019). Over the 2012–2017 period, Crocus simulations were fed by in situ measurements: air temperature, direct and diffuse shortwave incoming radiation, long-wave radiation, wind speed and direction, specific humidity, surface pressure, snow, and rain precipitation. Several snowpack variables (e.g., snow height, albedo and surface temperature, snow water equivalent and water output, snow energy balance components, snow density, and liquid water content) were simulated using Crocus for the study period considered here. These variables were exploited to distinguish the snow-melt phases. Simulated snow density and mass liquid water were used as inputs to compute P_s and for investigating the relationships with AP_s . Simulated snow variables and P_s were averaged over the upper 30 cm of the snowpack. This layer is the most important in terms of thermal and radiative properties (i.e., interaction with atmosphere, surface hoar formation, transmission of shortwave radiation, daily temperature cycles, variation in snow density and refreezing processes; Arenson et al., 2015; Burns et al., 2014; Fierz, 2011). Deeper in the snowpack, diurnal cycles of temperature are further dampened (Burns et al., 2014; Fierz, 2011).

2.5. Retrieval of Snow Properties From Apparent Thermal Inertia and Sensitivity Analysis

AP_s was compared with simulated snowpack variables to evaluate the role of each parameter in thermal inertia. In particular, we were interested in testing the relationship between AP_s and snow variables that affect snowpack's thermal properties, primarily snow density. Such analysis has been conducted using linear and nonlinear regressions models to identify the best empirical model.

Manual measurements of snow density ($n = 17$) were acquired in Torgnon between December 2012 and April 2016. They were compared with Crocus simulated snow density, and with snow density estimated using the empirical model developed starting from AP_s to validate the model.

Finally, a simplified sensitivity analysis was performed following Maltese, Bates, et al. (2013) to understand the sensitivity of AP_s to the range of variability of the albedo and the difference in day-night temperature, and to examine the uncertainty of snow density estimation from AP_s . AP_s was calculated by varying snow albedo and surface temperature within plausible ranges of values: α ranges from 0.6 to 0.95 with increment $\Delta\alpha = 0.05$ (–); ΔT ranges from 1 to 10 with increment $\Delta(\Delta T) = 0.2$ (K).

3. Results and Discussion

3.1. Toward the Use of Snow Thermal Inertia for Monitoring Snowmelt Processes

Results from Crocus simulations for all hydrological years allowed a first understanding of the snow dynamics at the investigated site. Figure 1 shows the time series of different variables modeled for the 2013–2014 season (all years analyzed in this study are shown in Figure S1): surface snow temperature (T_s , K), night-day temperature variation (ΔT_s , K), albedo (α , –), mean snow density of the upper 30 cm (ρ , kg/m³), snow depth (SD , m), snow water equivalent (SWE , mm), snow liquid water content (LWC , kg/m³), water output (i.e., *Snowmelt*, m²/s) and snow thermal inertia (P_s , J·m^{–2}·K^{–1}·s^{–1/2}). Multilayer Crocus data for LWC , T_s , ρ , and P_s are also shown in Figure 1.

The complex interactions between all these parameters allowed revealing the different phases of snow accumulation and melting. Accumulation periods and snow melting phases (i.e., warming, ripening, and output phases) were identified for each year mainly considering snow depth, surface temperature, snow density variation, liquid water content, and water output. Considering the winter 2013/2014, until the first week of March, surface temperature (T_s) is always below zero, and snow density (ρ) fluctuates around 250 kg/m³ (Figure 1b). We considered the marked drop in SD , associated with the rise of T_s and ρ as the main indicators of the start of melting period and the beginning of the warming phase (4 March 2014, Figure 1b; Dingman, 2015; McCreight & Small, 2014). In the second week of March, internal snowpack temperature gradually increases approaching the melting point, and snowpack becomes isothermal (around 18 March 2014, Figure 1f). During this time, a strong snow metamorphism occurs, density increases, and albedo consequently decreases. Depending on the atmospheric conditions, warming-freezing cycles could occur several times during snowmelt period. During the ripening phase, mean LWC of the snowpack increases, but water is retained in the snowpack and no snowmelt occurs (Figures 1d and 1e; Williams & Tarboton, 1999). During April, snow density reaches values of 500–600 kg/m³. The beginning of the output phase (3 April 2014) is marked by a sharp decrease in SWE and an increase in the production of melt water (i.e., *Snowmelt* in Figure 1d). Shaded areas in Figure 1 show the identified warming, ripening, and output phases. The behavior of thermal inertia is shown in Figures 1h and 2. P_s assumes values lower than 500 J·m^{–2}·K^{–1}·s^{–1/2} during the whole accumulation with a low variability within the snowpack. During the warming phase, P_s increases with increasing snow density. While during the ripening and output phases (when water appears on the surface) P_s reaches its highest values. During the melting period, P_s shows a greater variability in the upper layers (Figure 1h).

Figure 2 shows the behavior of AP_s and P_s modeled considering the upper 30 cm of snowpack across the same season. Considering all investigated years, P_s values vary between 20 and 900 J·m^{–2}·K^{–1}·s^{–1/2} for snow density ranging between 100 and 550 kg/m³. During the accumulation period in 2013 both P_s and AP_s show low and almost constant values. Throughout this period, high albedo values and large diurnal variability of surface temperature (Figure 1) generate low AP_s values, representing dry snow. Changes in surface temperature are likely due to fluctuation in air temperature, since fresh snow has a high porosity, and it behaves as an insulator. As the air temperature increases in spring, albedo decreases due to metamorphism and daily fluctuations in surface temperature are dampened. This process induces an increase in AP_s during March. During this phase, AP_s resembles P_s . AP_s continues to rise during the ripening phase, due to the ongoing gradual increase of snow density because of the formation of liquid water. In this phase, AP_s starts to diverge from P_s likely due to the appearance of liquid water content at surface. As the snow reaches its saturation point (maximum of LWC), snowmelt occurs, and AP_s and P_s reach maximum values

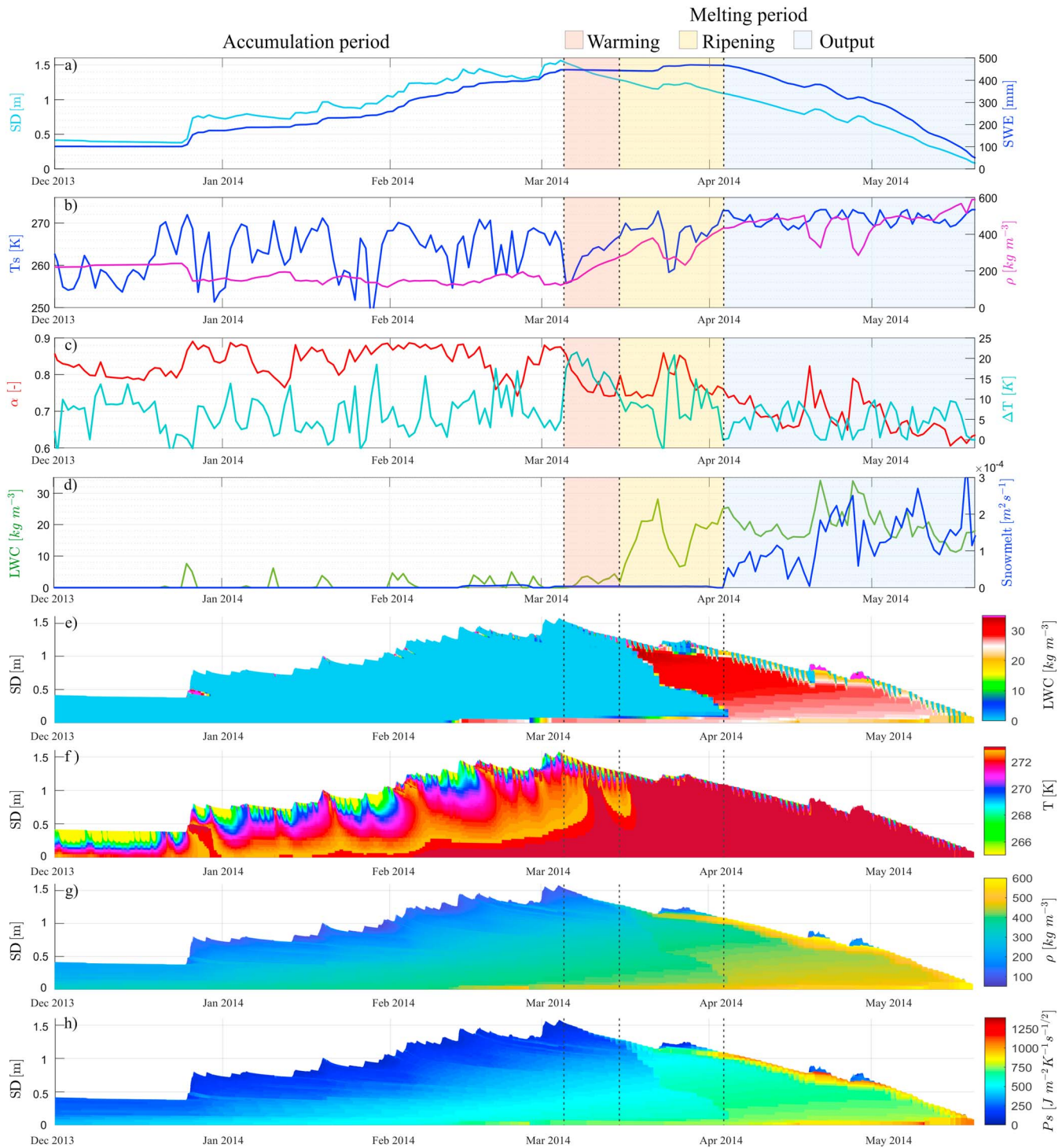


Figure 1. Seasonal time series of variables simulated with Crocus model for the hydrologic year 2013/2014 (the hydrological year ranges from the end of October to late May). Snow depth (SD), snow water equivalent (SWE), and *Snowmelt* are depicted as mean daily snowpack values, while density (ρ) and liquid water content (*LWC*) are computed as mean values in the upper 30 cm. T_s represents daily mean surface temperature, while ΔT is the temperature difference between 14.00 p.m. and 05.00 a.m. measurements. Albedo (α) was averaged between 13.00 and 15.00. Figures 1e–1h show the behavior of liquid water content (*LWC*), snow temperature (*T*), snow density (ρ), and snow thermal inertia (P_s) across the snow profile. Shaded red, yellow, and blue areas (and dotted lines) indicate warming, ripening, and output phases, respectively.

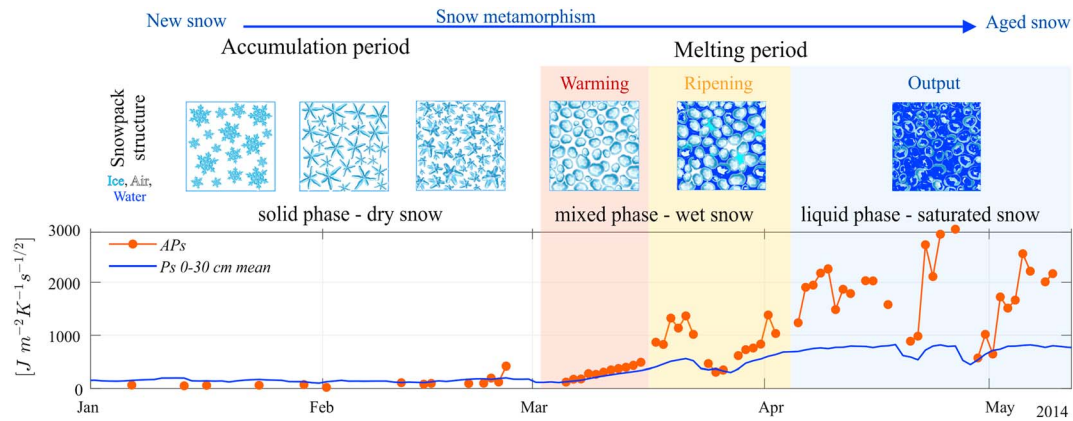


Figure 2. Apparent and thermal inertia of the alpine snowpack. Trend of P_s (blue line, mean of 0–30 cm) and AP_s (red line) for 2013–2014 hydrological year. P_s and AP_s have similar values during the snow season: Low values occur during the accumulation, an increase is observed during warming and ripening, and maximum values are reached in the output phase. Upper part shows the ideal evolution of the structure of the snowpack indicating changes in snow density and appearance of liquid water within snow.

corresponding to high and almost constant snow density (i.e., $\sim 500 \text{ kg/m}^3$). This ideal seasonal trend can be modified by a combination of snowfall events and snow melting. For example, one snow fall occurred at the end of March in 2014 induced a decline in AP_s and P_s due to the appearance of pristine snow. The decrease in AP_s values at the end of March can in fact be associated with fresh snow with density of 250 kg/m^3 and with a decrease in snow temperature with re-freezing of LWC . Hence, remotely sensed estimations of AP_s may be affected by rapid melting and refreeze processes that can occur during the melting period in seasonal snowpacks.

In an idealized sequence, AP_s could be described by a sigmoid function, with low values in the accumulation period, followed by a rise in warming and ripening phases and a subsequent stabilization, when the output phase starts. In this conceptual model it could be possible to define thresholds and metrics corresponding to snowmelt phases (e.g., the day of the year on which the melting season starts and the beginning of the output phase) and hence the possibility to discriminate dry, wet, and water-saturated snow from remote sensing of thermal inertia. In our case, mean values of AP_s are statistically different (in terms of t test) during accumulation, warming/ripening, and output phases (Figure 3b). While accumulation and output phases are clearly distinguishable from thermal inertia, the warming and ripening phases are often mixed together during the natural evolution of the snowpack, hence, they are hardly separable using the proposed method.

Overall, we found a good agreement between P_s and AP_s , with an R^2 of 0.74 (Figure S2). AP_s successfully reproduce P_s in the accumulation, warming, and ripening phase, while in the output phase we encountered a marked difference that could be due to the presence of surface layers of liquid water and changes of mass. The presence of materials with different thermal properties (water, air, ice, and LAPs) modifies the phase and amplitude of the fluctuation of daily surface temperature (Byrne & Davis, 1980), so that AP_s can diverge from the theoretical P_s model. In this context, underestimations in ΔT may occur in the output phase, and this may explain the higher values of AP_s with respect to P_s . Furthermore, simulated liquid water content from Crocus may be affected by errors (D’Amboise et al., 2017), and this can also explain the divergence between P_s and AP_s .

3.2. Estimation of Snow Density

A significant power law relationship between AP_s and simulated snow density was found for all the investigated years, both considering mean values of the whole snowpack ($R^2 = 0.71$, Figure 3a) and the upper 30 cm ($R^2 = 0.75$, data not shown). Worse results were instead found between AP_s and the other snowpack variables, such as SD ($R^2 = 0.05$), SWE ($R^2 = 0.04$), LWC ($R^2 = 0.25$), and snowmelt ($R^2 = 0.05$). Figure 3 indicates that AP_s can be used to provide estimation of mean snow density with a RMSE equal to 65 kg/m^3 . As a validation scheme of this model, we present a comparison between snow density estimated from AP_s with snow density measured in field (Figure S3). The goodness of fit of the regression ($R^2 = 0.8$; RMSE = 54 kg/m^3) further

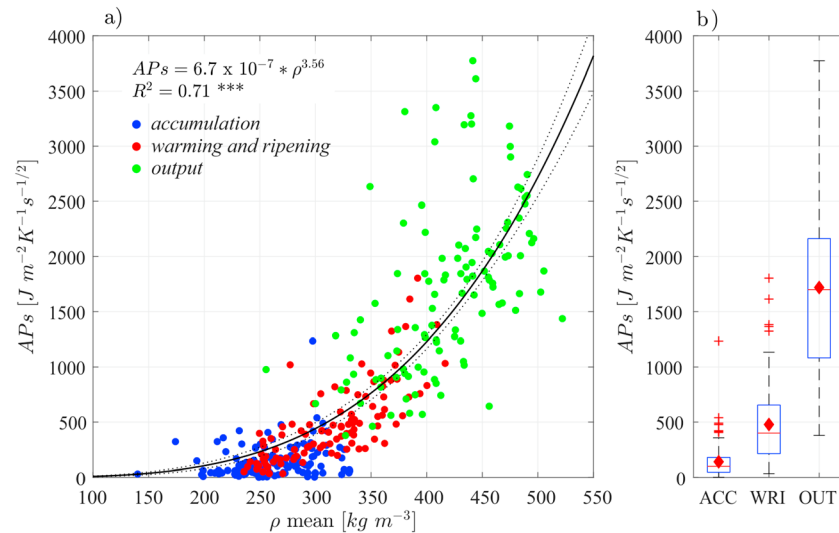


Figure 3. (a) Correlation between AP_s and mean snow density for all the investigated years (2012–2017). The regression is statistically significant ($p < 0.001$, $\alpha = 0.05$) and the 95% prediction boundary of the functions are represented. (b) Boxplot of AP_s values considering the different snow phases: accumulation (ACC, blue dots), warming and ripening (WRI, red dots), and output (OUT, green dots). Mean values differ statistically, what is confirmed by a t test with a significance level (α) of 0.05 and p -values always smaller than 0.001.

supports the reliability of the mean snow density retrieval from thermal inertia measurements. In our case, the ability of AP_s to estimate both mean snow density and upper 30 cm can be ascribed to the higher temporal variability of snow density with respect to the lower variability along the vertical profile.

During the different snow phases, AP_s assumes distinct values in all considered hydrological years (Figure 3b). AP_s values in the accumulation period are almost constant (i.e., average value around $147 J \cdot m^{-2} \cdot K^{-1} \cdot s^{-1/2}$ and standard deviation (st. dev.) equal to $147 J \cdot m^{-2} \cdot K^{-1} \cdot s^{-1/2}$, with average snow density of $246 kg/m^3$ and st. dev. equal to $36 kg/m^3$; during warming and ripening, AP_s assumes intermediate values (mean = 478, st. dev. = 355) and mean snow density of 310 (st. dev. = 45), while in the output phases mean values of AP_s are higher and more variable (mean = 1,719, st. dev. = 766), corresponding to highest snow density values (mean = 430, st. dev. = 60). During the melting period, part of the variability in the AP_s series may be due to the resurfacing of LAPs that induce a further decrease in snow albedo, increase in grain size, and a warming of the snowpack (Di Mauro et al., 2019). This may partially explain the higher scattering of data in Figure 3 and affect the correlation between AP_s and snow density.

Overall, these results indicate that average snow density can be estimated from thermal inertia. However, for the estimation of the SWE , both the knowledge of the mean value of the bulk snowpack density and snow depth are needed. In the future, the combination between optical/thermal data with passive and active microwave data may improve SWE estimation and snow monitoring.

Finally, results of the sensitivity analysis show that the uncertainty of snow density estimation from AP_s increases at low ΔT_s and α values (Figure S4). This is a typical condition occurring during ripening and output phases, when snow metamorphism decreases both α and ΔT_s . This analysis highlights the importance of precise surface temperature measurements to infer AP_s and snow density, especially during melting period. In the range of ΔT_s from 1.5 to 4 K, a precision of at least 0.2 K is necessary for obtaining variation in snow density estimation lower than $30 kg/m^3$. This corresponds to a variation $<10\%$ that is comparable with errors in manual measurements of snow density (Proksch et al., 2016).

4. Conclusions

In this paper, we introduce for the first time the use of snow thermal inertia in the context of snowmelt processes. In particular, we show that both P_s and AP_s assume distinct values during accumulation,

warming/ripening, and output phases, indicating that thermal inertia can potentially be used to provide information on snowpack conditions. Uncertainty factors that could influence APs estimations can be associated with instrumental accuracies, model assumptions, presence of liquid water and LAPs on surface snow, rapid snow dynamics (e.g., late snowfalls and melting), and cloud cover. Moreover, we provide first evidences that snow density can be successfully estimated from AP_s observations. The model was validated with independent snow density measurements. However, further studies are needed to consolidate and to extend our findings. Investigations with optical/thermal airborne sensors combined with field experiments and modeling tools are relevant to evaluate and interpret the spatial and temporal variability of AP_s in different geographic context and different snow/ice conditions.

Results presented in this study are of particular interest since AP_s is a variable that can be directly estimated from remotely sensed data. Thus, we believe that the use of snow thermal inertia may contribute to open new applications in Earth Observation and perspectives in the study of the cryosphere, as an example for snow hydrology and water resources management. The possibility to use APs to infer snow density could have significant impacts on snow hydrology studies, mainly for inferring the snow water equivalent. Currently, a strategy combining existing or future radar, optical and thermal missions could be defined with the perspective to specifically target a better estimation of the snow water equivalent, which is the parameter directly affecting the availability of water in the future.

Acknowledgments

The research was supported by the CHRISTMAS (Cryosphere High spatial Resolution Images and Snow/ice properties via apparent Thermal inertia obtained from Multispectral Advanced optical Systems) project funded by the Italian Space Agency (ASI). We thank S. Zoffoli (ASI) and all CHRISTMAS team for the discussion during the project. We thank G. Chirico and I. Cesana (UNIMB) for their input and A. Evdokimov who helped improve the manuscript. We are also grateful to the personnel of the Environmental Protection Agency of Aosta Valley (ARPA-VDA) for maintaining the experimental site in Torgnon (AO, Italy). We thank the two reviewers for the constructive comments on a previous version of the manuscript. CNRM/CEN is part of Labex OSUG@2020, (Investissements d'Avenir, grant agreement ANR-10-LABX-0056). The modeling work was funded by the French National Research Agency (ANR JCJC EBONI grant ANR-16-CE01-006). Observed and simulated data presented in this paper are available in the supporting information.

References

- Aït-Mesbah, S., Dufresne, J. L., Cheruy, F., & Hourdin, F. (2015). The role of thermal inertia in the representation of mean and diurnal range of surface temperature in semiarid and arid regions. *Geophysical Research Letters*, *42*, 7572–7580. <https://doi.org/10.1002/2015GL065553>
- Arenson, L. U., Colgan, W., & Marshall, H. P. (2015). *Physical, thermal, and mechanical properties of snow, ice, and permafrost. Snow and ice-related hazards, risks and disasters* (pp. 35–75). Oxford: Elsevier. <https://doi.org/10.1016/B978-0-12-394849-6.00002-0>
- Aubry-Wake, C., Baraer, M., McKenzie, J. M., Mark, B. G., Wigmore, O., Hellström, R., et al. (2015). Measuring glacier surface temperatures with ground-based thermal infrared imaging. *Geophysical Research Letters*, *42*, 8489–8497. <https://doi.org/10.1002/2015GL065321>
- Beniston, M., Farinotti, D., Stoffel, M., Andreassen, L. M., Coppola, E., Eckert, N., et al. (2018). The European mountain cryosphere: A review of its current state, trends, and future challenges. *The Cryosphere*, *12*(2), 759–794. <https://doi.org/10.5194/tc-12-759-2018>
- Beniston, M., Keller, F., & Goyette, S. (2003). Snow pack in the Swiss Alps under changing climatic conditions: An empirical approach for climate impacts studies. *Theoretical and Applied Climatology*, *74*(1–2), 19–31. <https://doi.org/10.1007/s00704-002-0709-1>
- Bormann, K. J., Brown, R. D., Derksen, C., & Painter, T. H. (2018). Estimating snow-cover trends from space. *Nature Climate Change*, *8*(11), 924–928. <https://doi.org/10.1038/s41558-018-0318-3>
- Brenning, A., Peña, M. A., Long, S., & Soliman, A. (2012). Thermal remote sensing of ice-debris landforms using ASTER: An example from the Chilean Andes. *The Cryosphere*, *6*(2), 367–382. <https://doi.org/10.5194/tc-6-367-2012>
- Brun, E., Martin, E., Simon, V., Gendre, C., & Coleou, C. (1989). An energy and mass model of snow cover suitable for operational avalanche forecasting. *Journal of Glaciology*, *35*(121), 333–342. <https://doi.org/10.1017/S002214300009254>
- Burns, S. P., Molotch, N. P., Williams, M. W., Knowles, J. F., Seok, B., Monson, R. K., et al. (2014). Snow temperature changes within a seasonal snowpack and their relationship to turbulent fluxes of sensible and latent heat. *Journal of Hydrometeorology*, *15*(1), 117–142. <https://doi.org/10.1175/JHM-D-13-026.1>
- Byrne, G. F., & Davis, J. R. (1980). Thermal inertia, thermal admittance, and the effect of layers. *Remote Sensing of Environment*, *9*(4), 295–300. [https://doi.org/10.1016/0034-4257\(80\)90035-8](https://doi.org/10.1016/0034-4257(80)90035-8)
- Calonne, N., Flin, F., Morin, S., Lesaffre, B., Du Roscoat, S. R., & Geindreau, C. (2011). Numerical and experimental investigations of the effective thermal conductivity of snow. *Geophysical Research Letters*, *38*, L23501. <https://doi.org/10.1029/2011GL049234>
- Champollion, N., Picard, G., Arnaud, L., Lefebvre, É., Macelloni, G., Rémy, F., & Fily, M. (2018). Marked decrease of the near surface snow density retrieved by AMSR-E satellite at Dome C, Antarctica, between 2002 and 2011. *The Cryosphere Discuss*, 1–32. <https://doi.org/10.5194/tc-2018-265>
- Cracknell, A. P., & Xue, Y. (1996). Thermal inertia determination from space—A tutorial review. *International Journal of Remote Sensing*, *17*(3), 431–461. <https://doi.org/10.1080/01431169608949020>
- Dadic, R., Mullen, P. C., Schneebeli, M., Brandt, R. E., & Warren, S. G. (2013). Effects of bubbles, cracks, and volcanic tephra on the spectral albedo of bare ice near the Transantarctic Mountains: Implications for sea glaciers on snowball Earth. *Journal of Geophysical Research: Earth Surface*, *118*, 1658–1676. <https://doi.org/10.1002/jgrf.20098>
- D'Amboise, C. J. L., Müller, K., Oxarango, L., Morin, S., & Schuler, T. V. (2017). Implementation of a physically based water percolation routine in the Crocus/SURFEX (V7.3) snowpack model. *Geoscientific Model Development*, *10*(9), 3547–3566. <https://doi.org/10.5194/gmd-10-3547-2017>
- Di Mauro, B., Baccolo, G., Garzonio, R., Giardino, C., Massabò, D., Piazzalunga, A., et al. (2017). Impact of impurities and cryoconite on the optical properties of the Morteratsch glacier (Swiss Alps). *The Cryosphere*, *11*(6), 2393–2409. <https://doi.org/10.5194/tc-11-2393-2017>
- Di Mauro, B., Fava, F., Ferrero, L., Garzonio, R., Baccolo, G., Delmonte, B., & Colombo, R. (2015). Mineral dust impact on snow radiative properties in the European Alps combining ground, UAV, and satellite observations. *Journal of Geophysical Research: Atmospheres*, *120*, 6080–6097. <https://doi.org/10.1002/2015JD023287>
- Di Mauro, B., Garzonio, R., Rossini, M., Filippa, G., Pogliotti, P., Galvagno, M., et al. (2019). Saharan dust events in the European Alps: role in snowmelt and geochemical characterization. *The Cryosphere*, *13*, 1147–1165. <https://doi.org/10.5194/tc-13-1147-2019>
- Dingman, S. L. (2015). *Physical hydrology* (p. 643). Waveland Press, Inc. ISBN: 1-4786-1118-9

- Dozier, J., & Painter, T. H. (2004). Multispectral and hyperspectral remote sensing of alpine snow properties. *Annual Review of Earth and Planetary Sciences*, 32(1), 465–494. <https://doi.org/10.1146/annurev.earth.32.101802.120404>
- Essery, R., Martin, E., Douville, H., Fernandez, A., & Brun, E. (1999). A comparison of four snow models using observations from an alpine site. *Climate Dynamics*, 15(8), 583–593. <https://doi.org/10.1007/s003820050>
- Fierz, C. (2011). Temperature profile of snowpack. In V. P. Singh, P. Singh, & U. K. Haritashya (Eds.), *Encyclopedia of Snow, Ice and Glaciers*. (Singh V.P) (pp. 1151–1154). Dordrecht: Springer. https://doi.org/10.1007/978-90-481-2642-2_569
- Gaitani, N., Burud, I., Thiis, T., & Santamouris, M. (2017). High-resolution spectral mapping of urban thermal properties with unmanned aerial vehicles. *Building and Environment*, 121, 215–224. <https://doi.org/10.1016/J.BUILDENV.2017.05.027>
- Galvagno, M., Wohlfahrt, G., Cremonese, E., Rossini, M., Colombo, R., Filipa, G., et al. (2013). Phenology and carbon dioxide source/sink strength of a subalpine grassland in response to an exceptionally short snow season. *Environmental Research Letters*, 8(2), 025008. <https://doi.org/10.1088/1748-9326/8/2/025008>
- Green, R. O., Dozier, J., Roberts, D., & Painter, T. (2002). Spectral snow-reflectance models for grain-size and liquid-water fraction in melting snow for the solar-reflected spectrum. *Annals of Glaciology*, 34(1), 71–73. <https://doi.org/10.3189/172756402781817987>
- Haerberli, W., & Whiteman, C. (2014). Snow and ice-related hazards, risks, and disasters, Chapter 2. <https://doi.org/10.1016/C2011-0-07024-2>
- Hall, D. K., & Martinec, J. (2012). *Remote sensing of ice and snow*. Dordrecht: Springer. <https://doi.org/https://doi.org/10.1007/978-94-009-4842-6>
- He, C., Liou, K. N., Takano, Y., Yang, P., Qi, L., & Chen, F. (2018). Impact of grain shape and multiple black carbon internal mixing on snow albedo: Parameterization and radiative effect analysis. *Journal of Geophysical Research: Atmospheres*, 123, 1253–1268. <https://doi.org/10.1002/2017JD027752>
- Huss, M., Bodo, B., Huggel, C., Jacobsen, D., Bradley, R. S., Clague, J. J., et al. (2017). Toward mountains without permanent snow and ice. *Earth's Future*, 5(5), 418–435. <https://doi.org/10.1002/2016EF000514>
- Immerzeel, W. W., van Beek, L. P. H., & Bierkens, M. F. P. (2010). Climate change will affect the Asian water towers. *Science*, 328(5984), 1382–1385. <https://doi.org/10.1126/science.1183188>
- Jonas, T., Marty, C., & Magnusson, J. (2009). Estimating the snow water equivalent from snow depth measurements in the Swiss Alps. *Journal of Hydrology*, 378(1–2), 161–167. <https://doi.org/10.1016/j.jhydrol.2009.09.021>
- Julitta, T., Cremonese, E., Migliavacca, M., Colombo, R., Galvagno, M., Siniscalco, C., et al. (2014). Using digital camera images to analyse snowmelt and phenology of a subalpine grassland. *Agricultural and Forest Meteorology*, 198, 116–125. <https://doi.org/10.1016/J.AGRFORMET.2014.08.007>
- Kahle, A. B., Gillespie, A. R., & Goetz, A. F. H. (1976). Thermal inertia imaging: A new geologic mapping tool. *Geophysical Research Letters*, 3(1), 26–28. <https://doi.org/10.1029/GL003i001p00026>
- Kang, J., Jin, R., Li, X., Ma, C., Qin, J., & Zhang, Y. (2017). High spatio-temporal resolution mapping of soil moisture by integrating wireless sensor network observations and MODIS apparent thermal inertia in the Babao River basin, China. *Remote Sensing of Environment*, 191, 232–245. <https://doi.org/10.1016/j.rse.2017.01.027>
- Kelly, R. E., Chang, A. T., Tsang, L., & Foster, J. L. (2003). A prototype AMSR-E global snow area and snow depth algorithm. *IEEE Transactions on Geoscience and Remote Sensing*, 41(2), 230–242. <https://doi.org/10.1109/TGRS.2003.809118>
- Kokhanovsky, A., Lamare, M., Di Mauro, B., Picard, G., Arnaud, L., Dumont, M., et al. (2018). On the reflectance spectroscopy of snow. *The Cryosphere*, 12(7), 2371–2382. <https://doi.org/10.5194/tc-12-2371-2018>
- Kokhanovsky, A. A., & Zege, E. P. (2004). Scattering optics of snow. *Applied Optics*, 43(7), 1589–1602. <https://doi.org/10.1364/AO.43.001589>
- König, M., Winther, J.-G., & Isaksson, E. (2001). Measuring snow and glacier ice properties from satellite. *Reviews of Geophysics*, 39(1), 1–27. <https://doi.org/10.1029/1999RG000076>
- Lacroix, P., Legresy, B., Remy, F., Blarel, F., Picard, G., & Brucker, L. (2009). Rapid change of snow surface properties at Vostok, East Antarctica, revealed by altimetry and radiometry. *Remote Sensing of Environment*, 113(12), 2633–2641. <https://doi.org/10.1016/j.rse.2009.07.019>
- Leduc-Leballeur, M., Picard, G., Macelloni, G., & Brogioni, M. (2017). IEEE NS and HM: Snowmelt in Antarctica as derived from SMOS observations. In 2017 IEEE International Geoscience and Remote Sensing Symposium (IGARSS) (pp. 2829–2831). IEEE. <https://doi.org/10.1109/IGARSS.2017.8127587>
- Lemmetyinen, J., Schwank, M., Rautiainen, K., Kontu, A., Parkkinen, T., Mätzler, C., et al. (2016). Snow density and ground permittivity retrieved from L-band radiometry: Application to experimental data. *Remote Sensing of Environment*, 180, 377–391. <https://doi.org/10.1016/j.rse.2016.02.002>
- Libois, Q., Picard, G., France, J. L., Arnaud, L., Dumont, M., Carmagnola, C. M., & King, M. D. (2013). Influence of grain shape on light penetration in snow. *The Cryosphere*, 7(6), 1803–1818. <https://doi.org/10.5194/tc-7-1803-2013>
- Liou, K. N., Takano, Y., He, C., Yang, P., Leung, L. R., Gu, Y., & Lee, W. L. (2014). Stochastic parameterization for light absorption by internally mixed BC/dust in snow grains for application to climate models. *Journal of Geophysical Research: Atmospheres*, 119, 7616–7632. <https://doi.org/10.1002/2014JD021665>
- Maltese, A., Bates, P. D., Capodici, F., Cannarozzo, M., Ciraolo, G., & La Loggia, G. (2013). Critical analysis of thermal inertia approaches for surface soil water content retrieval. *Hydrological Sciences Journal*, 58(5), 1144–1161. <https://doi.org/10.1080/02626667.2013.802322>
- Maltese, A., Capodici, F., Ciraolo, G., & La Loggia, G. (2013). Mapping soil water content under sparse vegetation and changeable sky conditions: Comparison of two thermal inertia approaches. *Journal of Applied Remote Sensing*, 7(1), 073548. <https://doi.org/10.1117/1.JRS.7.073548>
- Maltese, A., Capodici, F., Corbari, C., Ciraolo, G., Loggia, G. L., & Sobrino, J. A. (2012). Critical analysis of the thermal inertia approach to map soil water content under sparse vegetation and changeable sky conditions. In Proceedings of SPIE - the International Society for Optical Engineering. <https://doi.org/10.1117/12.975676>
- McCreight, J. L., & Small, E. E. (2014). Modeling bulk density and snow water equivalent using daily snow depth observations. *The Cryosphere*, 8(2), 521–536. <https://doi.org/10.5194/tc-8-521-2014>
- Migliavacca, M., Galvagno, M., Cremonese, E., Rossini, M., Meroni, M., Sonnentag, O., et al. (2011). Using digital repeat photography and eddy covariance data to model grassland phenology and photosynthetic CO₂ uptake. *Agricultural and Forest Meteorology*, 151(10), 1325–1337. <https://doi.org/10.1016/J.AGRFORMET.2011.05.012>
- Minacapilli, M., Iovino, M., & Blanda, F. (2009). High resolution remote estimation of soil surface water content by a thermal inertia approach. *Journal of Hydrology*, 379(3–4), 229–238. <https://doi.org/10.1016/j.jhydrol.2009.09.055>

- Mitra, D. S., & Majumdar, T. J. (2004). Thermal inertia mapping over the Brahmaputra basin, India using NOAA-AVHRR data and its possible geological applications. *International Journal of Remote Sensing*, *25*(16), 3245–3260. <https://doi.org/10.1080/01431160310001632701>
- Molotch, N. P., Colee, M. T., Bales, R. C., & Dozier, J. (2005). Estimating the spatial distribution of snow water equivalent in an alpine basin using binary regression tree models: The impact of digital elevation data and independent variable selection. *Hydrological Processes*, *19*(7), 1459–1479. <https://doi.org/10.1002/hyp.5586>
- Naderpour, R., & Schwank, M. (2018). Snow wetness retrieved from L-band radiometry. *Remote Sensing*, *10*(3), 359. <https://doi.org/10.3390/rs10030359>
- Naderpour, R., Schwank, M., Mätzler, C., Lemmetyinen, J., & Steffen, K. (2017). Snow Density and Ground Permittivity Retrieved From L-Band Radiometry: A Retrieval Sensitivity Analysis. *IEEE Journal of Selected Topics in Applied Earth Observations and Remote Sensing*, *10*(7), 3148–3161. <https://doi.org/10.1109/JSTARS.2017.2669336>
- Nearing, G. S., Moran, M. S., Scott, R. L., & Ponce-Campos, G. (2012). Coupling diffusion and maximum entropy models to estimate thermal inertia. *Remote Sensing of Environment*, *119*, 222–231. <https://doi.org/10.1016/j.rse.2011.12.012>
- Nolin, A. W. (2010). Recent advances in remote sensing of seasonal snow. *Journal of Glaciology*, *56*(200), 1141–1150. <https://doi.org/10.3189/002214311796406077>
- Oerlemans, J. (1994). Quantifying global warming from the retreat of glaciers. *Science*, *264*(5156), 243–245. <https://doi.org/10.1126/science.264.5156.243>
- Painter, T. H., Barrett, A. P., Landry, C. C., Neff, J. C., Cassidy, M. P., Lawrence, C. R., et al. (2007). Impact of disturbed desert soils on duration of mountain snow cover. *Geophysical Research Letters*, *34*, L12502. <https://doi.org/10.1029/2007GL030284>
- Painter, T. H., Bryant, A. C., & Skiles, S. M. (2012). Radiative forcing by light absorbing impurities in snow from MODIS surface reflectance data. *Geophysical Research Letters*, *39*, L17502. <https://doi.org/10.1029/2012GL052457>
- Painter, T. H., Seidel, F. C., Bryant, A. C., McKenzie Skiles, S., & Rittger, K. (2013). Imaging spectroscopy of albedo and radiative forcing by light-absorbing impurities in mountain snow. *Journal of Geophysical Research: Atmospheres*, *118*, 9511–9523. <https://doi.org/10.1002/jgrd.50520>
- Pomeroy, J., & Brun, E. (2001). Physical properties of snow. Snow ecology: An interdisciplinary examination of snow-covered ecosystems. <https://doi.org/10.1017/CBO9781107415324.004>
- Price, J. C. (1977). Thermal inertia mapping: A new view of the Earth. *Journal of Geophysical Research*, *82*(18), 2582–2590. <https://doi.org/10.1029/JC082i018p02582>
- Price, J. C. (1980). The potential of remotely sensed thermal infrared data to infer surface soil moisture and evaporation. *Water Resources Research*, *16*(4), 787–795. <https://doi.org/10.1029/WR016i004p00787>
- Proksch, M., Rutter, N., Fierz, C., & Schneebeli, M. (2016). Intercomparison of snow density measurements: Bias, precision, and vertical resolution. *The Cryosphere*, *10*(1), 371–384. <https://doi.org/10.5194/tc-10-371-2016>
- Putzig, N. E., & Mellon, M. T. (2007). Apparent thermal inertia and the surface heterogeneity of Mars. *Icarus*, *191*(1), 68–94. <https://doi.org/10.1016/j.icarus.2007.05.013>
- Roy, A., Toose, P., Williamson, M., Rowlandson, T., Derksen, C., Royer, A., et al. (2017). Response of L-band brightness temperatures to freeze/thaw and snow dynamics in a prairie environment from ground-based radiometer measurements. *Remote Sensing of Environment*, *191*, 67–80. <https://doi.org/10.1016/j.rse.2017.01.017>
- Schellenberger, T., Ventura, B., Zebisch, M., & Notarnicola, C. (2012). Wet snow cover mapping algorithm based on multitemporal COSMO-SkyMed X-band SAR images. *IEEE Journal of Selected Topics in Applied Earth Observations and Remote Sensing*, *5*(3), 1045–1053. <https://doi.org/10.1109/JSTARS.2012.2190720>
- Schwank, M., Mätzler, C., Wiesmann, A., Wegmüller, U., Pulliainen, J., Lemmetyinen, J., et al. (2015). Snow density and ground permittivity retrieved from L-band radiometry: A synthetic analysis. *IEEE Journal of Selected Topics in Applied Earth Observations and Remote Sensing*, *180*(8), 377–391. <https://doi.org/10.1016/j.rse.2016.02.002>
- Schwank, M., & Naderpour, R. (2018). Snow density and ground permittivity retrieved from L-band radiometry: Melting effects. *Remote Sensing*, *10*(3), 354. <https://doi.org/10.3390/rs10020354>
- Sergienko, O. V., Douglas, R. M. A. Y. E. A. L., & Thom, J. E. (2008). Reconstruction of snow/firn thermal diffusivities from observed temperature variation: Application to icebergs C16, Ross Sea, Antarctica, 2004–07. *Annals of Glaciology*, *49*, 91–95. <https://doi.org/10.3189/172756408787814906>
- Shi, J., & Dozier, J. (2000). Estimation of snow water equivalence using SIR-C/X-SAR. I. Inferring snow density and subsurface properties. *IEEE Transactions on Geoscience and Remote Sensing*, *2017*(6), 1–17. <https://doi.org/10.1155/2017/8739598>
- Short, N. M., & Stuart, L. M. J. (1982). In N. M. Short & L. M. Stuart, Jr. (Eds.), *The Heat Capacity Mapping Mission (HCMM) anthology*. NASA SP-465, (p. 264). Washington, D.C: NASA.
- Skiles, S. M., Flanner, M., Cook, J. M., Dumont, M., & Painter, T. H. (2018). Radiative forcing by light-absorbing particles in snow. *Nature Climate Change*, *8*(11), 964–971. <https://doi.org/10.1038/s41558-018-0296-5>
- Snehmani, Venkataraman, G., Nigam, A. K., & Singh, G. (2010). Development of an inversion algorithm for dry snow density estimation and its application with ENVISAT-ASAR dual co-polarization data. *Geocarto International*, *25*(8), 597–616. <https://doi.org/10.1080/10106049.2010.516843>
- Stiles, W. H., & Ulaby, F. T. (1980). The active and passive microwave response to snow parameters: 1. Wetness. *Journal of Geophysical Research*, *85*(C2), 1037. <https://doi.org/10.1029/JC085iC02p01037>
- Sturm, M., Taras, B., Liston, G. E., Derksen, C., Jonas, T., & Lea, J. (2010). Estimating snow water equivalent using snow depth data and climate classes. *Journal of Hydrometeorology*, *11*(6), 1380–1394. <https://doi.org/10.1175/2010JHM1202.1>
- Tedesco, M. (2014). *Remote sensing of the cryosphere*. Wiley-Blackwell. <https://doi.org/10.1002/9781118368909> ISBN:9781118368909
- Thakur, P. K., Aggarwal, S. P., Garg, P. K., Garg, R. D., Mani, S., Pandit, A., & Kumar, S. (2012). Snow physical parameters estimation using space-based synthetic aperture radar. *Geocarto International*, *27*(3), 263–288. <https://doi.org/10.1080/10106049.2012.672477>
- Tian, J., Su, H., He, H., & Sun, X. (2015). An empirical method of estimating soil thermal inertia. *Advances in Meteorology*, *2015*, 1–9. <https://doi.org/10.1155/2015/428525>
- Tuzet, F., Dumont, M., Lafaysse, M., Picard, G., Arnaud, L., Voisin, D., et al. (2017). A multilayer physically based snowpack model simulating direct and indirect radiative impacts of light-absorbing impurities in snow. *The Cryosphere*, *11*(6), 2633–2653. <https://doi.org/10.5194/tc-11-2633-2017>
- Ulaby, F. T., & Stiles, W. H. (1980). The active and passive microwave response to snow parameters: 2. Water equivalent of dry snow. *Journal of Geophysical Research*, *85*(C2), 1045. <https://doi.org/10.1029/JC085iC02p01045>

- Van Doninck, J., Peters, J., De Baets, B., De Clercq, E. M., Ducheyne, E., & Verhoest, N. E. C. (2011). The potential of multitemporal Aqua and Terra MODIS apparent thermal inertia as a soil moisture indicator. *International Journal of Applied Earth Observation and Geoinformation*, 13(6), 934–941. <https://doi.org/10.1016/j.jag.2011.07.003>
- Verhoef, A. (2004). Remote estimation of thermal inertia and soil heat flux for bare soil. *Agricultural and Forest Meteorology*, 123(3–4), 221–236. <https://doi.org/10.1016/j.agrformet.2003.11.005>
- Verseghy, D. L. (1991). Class—A Canadian land surface scheme for GCMS. I. Soil model. *International Journal of Climatology*, 11(2), 111–133. <https://doi.org/10.1002/joc.3370110202>
- Verstraeten, W. W., Veroustraete, F., Van Der Sande, C. J., Grootaers, I., & Feyen, J. (2006). Soil moisture retrieval using thermal inertia, determined with visible and thermal spaceborne data, validated for European forests. *Remote Sensing of Environment*, 101(3), 299–314. <https://doi.org/10.1016/j.rse.2005.12.016>
- Vionnet, V., Brun, E., Morin, S., Boone, A., Faroux, S., Le Moigne, P., et al. (2012). The detailed snowpack scheme Crocus and its implementation in SURFEX v7.2. *Geoscientific Model Development*, 5(3), 773–791. <https://doi.org/10.5194/gmd-5-773-2012>
- Wang, J., Bras, R. L., Sivandran, G., & Knox, R. G. (2010). A simple method for the estimation of thermal inertia. *Geophysical Research Letters*, 37, W12525. <https://doi.org/10.1029/2009GL041851>
- Warren, S. G. (1982). Optical properties of snow. *Reviews of Geophysics*, 20(1), 67. <https://doi.org/10.1029/RG020i001p00067>
- Warren, S. G., & Wiscombe, W. J. (1980). A Model for the Spectral Albedo of Snow. II: Snow Containing Atmospheric Aerosols. *Journal of the Atmospheric Sciences*, 37(12), 2734–2745. [https://doi.org/10.1175/1520-0469\(1980\)037<2734:AMFTSA>2.0.CO;2](https://doi.org/10.1175/1520-0469(1980)037<2734:AMFTSA>2.0.CO;2)
- Williams, K. S., & Tarboton, D. G. (1999). The ABC's of snowmelt: A topographically factorized energy component snowmelt model. *Hydrological Processes*, 13(12–13), 1905–1920. [https://doi.org/10.1002/\(SICI\)1099-1085\(199909\)13:12/13<1905::AID-HYP890>3.0.CO;2-#](https://doi.org/10.1002/(SICI)1099-1085(199909)13:12/13<1905::AID-HYP890>3.0.CO;2-#)
- Xue, Y., & Cracknell, A. P. (1995). Advanced thermal inertia modelling. *International Journal of Remote Sensing*, 16(3), 431–446. <https://doi.org/10.1080/01431169508954411>